International Journal of Optomechatronics
Publication details, including instructions for authors and subscription information:
http://www.informaworld.com/smpp/title~content=t741771165

Laser-Induced Thermocapillary Convection for Mesoscale Manipulation

Emir Vela [ab]; Moustapha Hafez [a]; Stéphane Régnier [b]
[a] CEA LIST, Sensory Interfaces Laboratory, Fontenay-aux-Roses, France [b] Institut des Systèmes Intelligents et Robotique (ISIR), Université Pierre et Marie Curie/CNRS, Paris, France

Online publication date: 20 November 2009

To cite this Article Vela, Emir, Hafez, Moustapha and Régnier, Stéphane(2009) 'Laser-Induced Thermocapillary Convection for Mesoscale Manipulation', International Journal of Optomechatronics, 3: 4, 289 — 302
To link to this Article: DOI: 10.1080/15599610903389477
URL: http://dx.doi.org/10.1080/15599610903389477

International Journal of Optomechatronics, 3: 289–302, 2009

ISSN: 1559-9612 print/1559-9620 online
DOI: 10.1080/15599610903389477

LASER-INDUCED THERMOCAPILLARY CONVECTION FOR MESOSCALE MANIPULATION

Emir Vela[1,2], Moustapha Hafez[1], and Stéphane Régnier[2]
[1]*CEA LIST, Sensory Interfaces Laboratory, Fontenay-aux-Roses, France*
[2]*Institut des Systèmes Intelligents et Robotique (ISIR), Université Pierre et Marie Curie/CNRS, Paris, France*

Modulation of surface stresses is a recent and promising method to perform mesoscale manipulation of components in liquid medium. We present a promising approach using infra red laser-induced thermocapillary-driven flow for handling multiple or single large and heavy objects. The objects are immersed in thin liquid layers and in contact with the substrate surface. These objects can be handled with high speed thermocapillary convection flow reaching significant forces depending on the object sizes. Velocity measurements showed that 92 µm-sized spherical beads can be dragged with velocities of about 5.5 mm/s. Parallel non-contact micromanipulation can be achieved.

Keywords: Marangoni effect, mesoscale, micromanipulation, surface tension, thermocapillary

1. INTRODUCTION

There is currently a challenging need for techniques which can manipulate mesoscale objects and components. A large amount of research is underway in this field, searching for flexible and versatile mesoscale manipulation techniques that can be used in the hybrid electronic, microsystem, and biomedical industries.

Such applications are beyond the limits of pick-and-place techniques, such as microgrippers (Millet et al. 2004) and cantilevers (Haliyo et al. 2006), because at this scale they become too time-consuming. There are also significant difficulties for manipulation due to the dominant effect of surface forces (Lambert and Régnier 2006), and there is a high risk of sample contamination.

Recent developments have focused on massive, multiple and parallel mesoscale manipulation methods for improving speed and reducing the high cost of pick-and-place techniques. However, non-contact methods are more suitable for this kind of manipulation and a number of techniques are being investigated using different types of driving force, such as optical tweezers (Arai et al. 2004; Curtis et al. 2002), electric fields (Moesner and Higuchi 1997; Chiou et al. 2005), magnetic fields (Assi et al. 2002); and microfluidic systems (Chung et al. 2008). Each of these techniques is limited to specific types of objects. For example, to achieve precise manipulation

Address correspondence to Emir Vela, CEA LIST, Sensory Interfaces Laboratory, 18 route du Panorama BP6, 92265 Fontenay-aux-Roses, France. E-mail: emir.vela-saavedra@cea.fr

NOMENCLATURE

Bo_D	Dynamic Bond number	β	thermal expansion
F	force	γ	coefficient of friction
L	characteristic length	η	dynamic viscosity
Ma	Marangoni number	κ	thermal diffusivity
Ra	Rayleigh number	ν	kinematic viscosity
T	temperature	ρ	density
V	volume	σ	surface tension
a	bead acceleration	σ_T	temperature derivative of surface tension
g	gravitational acceleration		
k	thermal conductivity	τ	shear stress
u_x	horizontal velocity		

using optical tweezers the object being moved must be transparent and have a spherical shape. When using (di)electrophoresis techniques, the particles need to be dielectric or conductive, the electrodes have to be patterned in specific positions, and, in order to attain high resolution, the electrodes have to be numerous and spaced sufficiently close together; hence, a large number of connecting wires are required.

Another recent and promising method is microfluidic actuation by modulation of surface stresses (Kataoka and Troian 1999; Darhuber and Troian 2005). In this case, fluid motion is driven by altering the surface tension of the fluid interfaces.

Droplet manipulation by modulation of surface tension is now a broad area of research. Droplets are used as carriers for chemical substances, or even microcomponents, to perform reactions, mixing or self-assembly. Droplet manipulation by electrowetting on dielectrics (EWOD) was accomplished by Pollack et al. (2000). In this process, surface tension is controlled by an electric field applied at one edge of the droplet by activating an electrode patterned onto a substrate. Similarly, Darhuber et al. (2003) manipulated droplets approximately 1 mm in diameter using the thermocapillary effect. A surface tension gradient was generated at the droplet interface by heat conduction from microheaters patterned onto a substrate. Thus, the droplet moves toward the colder region. More recently, Baroud et al. (2007) and Cordero et al. (2008) used thermocapillary effects to manipulate oil droplets transported by a water flow in microfabricated PDMS channels. Heating one side of the oil droplet-water interface with a focused 1480 nm infra red (IR) laser, droplets can be stopped, sorted, or moved in parallel. Ohta et al. (2007) demonstrated another interesting technique for micromanipulation. Air bubbles within oil can be dragged by creating a thermal gradient onto a light absorbing substrate. The thermal gradient is transferred from the absorbing substrate to the fluid medium that can vary for different applications. Thus, a surface tension gradient is imparted at the fluid-substrate interface. This drives fluid motion that drags the air bubbles.

Basu and Gianchandani (2007) demonstrated micromanipulation with localized fluid actuation by shaping thermocapillary flow, or "Marangoni flow", in thin free surface liquid layers. This flow is driven by temperature perturbation of surface tension using a micro heat source positioned above the liquid-air interface

(free surface). Toroidal flows can be shaped, which are centred at the heat source position. With this method, suspended microparticles of up to 30 μm in size and water droplets in oil can be manipulated without the need for microfabricated structures on substrates (Basu and Gianchandani 2008).

None of the non-contact methods discussed above performed the manipulation of mesoscale objects having random properties (shapes and compositions).

In this article, we present a promising approach to mesoscale manipulation based on a highly localized thermocapillary effect, or Bénard–Marangoni convection, in thin free surface liquid layers heated from below with a focused 1480 nm IR laser.

Here, the flow generated is toroidal-shaped and centered at the focal point of the laser, allowing heavy and random-shaped mesoscale objects (not only droplets or bubbles but also glass beads) to be dragged. The flow drags these objects, which are totally immersed and in contact with the substrate, toward the laser's focal point. The principle of precise and controlled manipulation on a non-patterned substrate of multiple or single mesoscale objects ranging from 30 up to 300 μm in size, was reported in a previous publication (Vela et al. 2008). In this work, we demonstrate that the main and dominant phenomenon generating fluid motion is the thermocapillary effect. We present velocity measurements of micro-beads motion using a high-speed camera. Finally, the magnitude of the fluidic forces acting on the beads are estimated.

2. MANIPULATION WORKING PRINCIPLE

At the mesoscale, surface forces are greater than volume forces. For instance, a scaling law gives a ratio between these forces which is proportional to L^{-1}. Taking $L = 400\,\mu\text{m}$ as a characteristic length, this ratio has a magnitude on the scale of $10^3/\text{m}$.

Hence, surface forces are more suitable for manipulation at this scale. In this contribution, surface tension forces are used to move meso-sized objects immersed in liquid.

2.1. Dimensionless Analysis

Two phenomena are likely to occur when a thin fluid layer is heated from below. The first is natural or free convection. As the temperature increases, the liquid density becomes smaller and rises up. The cooler and heavier fluid that is located above goes down. This convection is produced under the influence of gravity (inertial effect). The second phenomenon is thermocapillary convection which is explained in detail in the next section.

Within a shallow depth of liquid, natural convection becomes negligible compared to thermocapillary convection, as the latter becomes the dominant mechanism.

Microfluidic analysis, using dimensionless numbers, can be used to determine which type of convection will dominate. Dimensionless numbers is a practical way to assess the relative significance of phenomena in microfluidics, as they express the ratios between competing phenomena. The dimensionless numbers used and

Table 1. Dimensionless fluidic numbers

Dimensionless Numbers			Water
Bo_D	$\rho g L^2/\sigma_T \Delta T$	Buoyant/surface tension forces	3.81×10^{-4}
Ma	$-\frac{\partial \sigma}{\partial T}\frac{\Delta T L}{\kappa \eta}$	Surface tension/viscous forces	2.14×10^4
Ra	$g\beta \Delta T L^3/\nu^2$	Buoyant/viscous forces	6.59

their computed values for liquid water are listed in Table 1. The Marangoni (Ma) and Rayleigh (Ra) numbers express the ratio between the surface tension forces and viscous forces, and between the buoyancy forces, and viscous forces, respectively. Taking a characteristic length of $L = 400\,\mu m$, a value that is equal to the water depth used in most experiments, and an estimated $\Delta T = 50\,K$, a value of $Ma = 1.61 \times 10^4$ is obtained. To estimate ΔT, we referred to Hollis et al. (1996), where a calculation of ΔT was presented for a similar IR laser (1480 nm, 40 mW). A temperature of 358 K was found at the focal point in water medium. Considering a room temperature of 298 K, at worst $\Delta T = 60\,K$ is set between the bottom and free surface of the water layer. So by comparison with our set up, $\Delta T = 50\,K$ was taken for our calculations. When Ma is greater than a critical value, $Ma_c = 81$, a hydrodynamic instability appears (Maroto et al. 2007). The ratio between Ra and Ma (the dynamic Bond number Bo_D) gives $Bo_D = 1.73 \times 10^{-4}$, so Ma is a factor of 10^4 larger than the Rayleigh number. In such a case, the dominant mechanism is Marangoni convection. In fact, Bo_D is proportional to L^2. We can therefore see that for thin liquid layers, free convection is negligible in comparison to the Marangoni effect. Table 2 summarizes the thermophysical properties of liquid water used here. Having performed this analysis, we will assume going forward that Marangoni convection is the mechanism that drives the flow and the manipulation principle described is based on this mechanism. Formulation of the boundary conditions for this effect is described in the next section.

2.2. Thermocapillary or Bénard–Marangoni Convection

Variations in surface tension at the interface between two immiscible fluids cause an imbalance in the shear stress, which in turn causes fluid motion to arise at

Table 2. Physical properties of liquid water at 20°C (Squires and Quake 2005)

Parameter	Unity	Value
ρ	kg/m^3	1000
η	Ns/m^2	1.0×10^{-3}
ν	m^2/s	1.0×10^{-6}
k	$W/m \times K$	0.6
κ	m^2/s	1.4×10^{-7}
σ	N/m	73×10^{-3}
σ_T	$N/m \times K$	-0.15×10^{-3}
β	1/K	2.1×10^{-4}

the interface. A surface tension gradient can be generated by locally heating from below using absorption of an IR laser (1480 nm) in a thin liquid layer (<1 mm) that is in direct contact with air. The surface tension gradient is imparted when the laser or the heat transferred from below reaches the interface. This gives rise to a shear stress gradient and a resultant motion of the fluid. This motion arises in cold regions located away from the laser beam axis and draws liquid from the warm regions. This phenomenon can be explained in terms of the decrease of cohesion forces that is caused by the temperature increase near the laser axis, while within colder regions cohesion forces remain larger. Figure 1 illustrates this principle. This type of convective flow is known as surface-tension-driven, Bénard-Marangoni or thermocapillary convection. In Figure 1*a*, a toroidal convective cell is established due to the surface tension gradient. At the free surface, the flow is directed away from the laser beam axis because cold regions draw the liquid from hot regions. At the bottom near the glass substrate, the flow is directed toward the laser beam creating a recirculation zone while maintaining an overall null net flow for the convective micro-fluid system. Figure 1*b* depicts the flow velocity profile (DaCosta 1993) and an immersed micro-bead that is dragged by the subsurface flow toward the laser focus. This is the principle that we use to manipulate meso-sized beads in the size range from 30–300 μm.

2.3. Formulation

In fluid mechanics, the shear stress is proportional to the strain rate and the coefficient of proportionality is the viscosity of the fluid. In Eq. (1) this proportionality is given for a Newtonian fluid.

$$\tau = \eta \frac{\partial u_x}{\partial y} \tag{1}$$

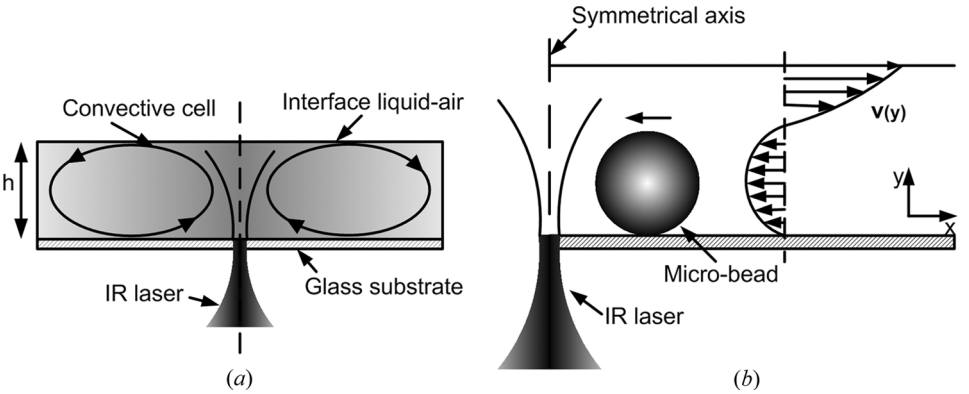

Figure 1. Principle of thermocapillary manipulation. (*a*) IR laser absorption heats a thin film of liquid from below, therefore a convective flow is generated by a surface tension gradient and (*b*) Velocity profile of the convection flow in a thin liquid layer heated from below. A micro-bead immersed within the liquid is reached by a velocity profile that drags it toward the laser focus. The arrow above the bead represents the motion direction.

where u_x is the horizontal velocity and y is the vertical coordinate (see Figure 1*b*). If we set the viscous stresses equal to the thermocapillary stresses at the liquid-air interface, Eq. (2) is obtained.

$$\tau = \eta \frac{\partial u_x}{\partial y} = \frac{\partial \sigma}{\partial T} \frac{\partial T}{\partial x} \tag{2}$$

where $\frac{\partial \sigma}{\partial T}$ is the temperature derivative of surface tension σ_T. Eq. (2) highlights the fact that shear stress depends on the temperature gradient due to the temperature dependence of surface tension. $\sigma_T < 0$ for most liquids and is taken as a constant in this work. This is a valid assumption since when the temperature is lower than a critical temperature T_c, the surface tension dependence on the temperature is near-linear and can be computed by Eotvo's law (Adamson and Gast 1997). Ramsay and Shields (1893) have adjusted the Eotvo's relationship by replacing the critical temperature T_c by $T_c - 6$, since at this temperature the surface tension is close to zero, giving $\sigma V_m^{2/3} = k_e(T_c - 6 - T)$, where V_m is the molar volume and k_e is a constant with a value of about 2.1×10^{-7} Nm/K for most liquids. We can see from this relationship that the surface tension varies linearly with respect to temperature, and by computing the derivative the value of σ_T is found.

The equations governing fluid motion during heating with a laser beam for Marangoni convection were reported in Longtin et al. (1999). These equations represent conservation of mass, Navier–Stokes or conservation of momentum, conservation of thermal energy, and the respective boundary conditions for taking Eq. (2) at the fluid interface where $y = h =$ liquid depth.

3. APPARATUS AND EXPERIMENTS

The experimental set up consisted of an inverted Olympus microscope IX71 with a microscope objective (4×, NA = 0.1, $f = 20$ mm), a high speed DALSA Genie Monochrome CMOS camera (1", 1400×1024 pixels, 60 fps), an IR laser (1480 nm, 120 mW), and a 2-degrees of freedom (DOF) mirror scanner. The laser power after passing through optical elements was about 80 mW at the focal point. The calculated laser intensity was about 17340 W/cm^2. The laser absorption in water was about 31.29 mW (absorption coefficient of water of 2345/m). The sample holder was a petri dish (soda-lime-glass, 60 mm diameter and 12 mm height) with liquid water filled to a specified depth <0.8 mm. Microparticles were deposited into the thin water layer.

Figure 2 shows the experimental set up. The IR laser beam is directed to the sample by a dichroic mirror scanner through a microscope objective (MO). The beads are dragged by the flow generated by laser scanning of the sample and follow the laser focus. The manipulation process was monitored by a high speed camera. The 2-DOF mirror scanner is a compact mechatronic system actuated by four electromagnets in a push-pull configuration.

Sample preparation is an important step for ensuring experimental reproducibility. The petri dish was first cleaned with distilled water and then dried. Isopropanol was added and left for at least three minutes to remove any possible organic material. The isopropanol was then removed and the petri dish dried with pure and dry gas.

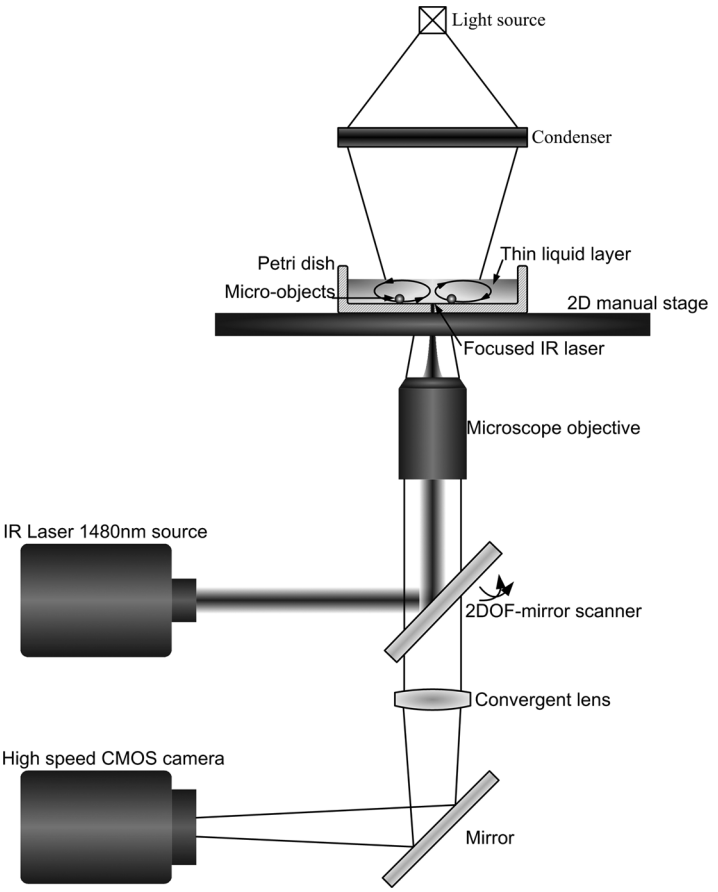

Figure 2. Experimental apparatus scheme for mesoscale manipulation. An IR laser 1480 nm is directed by a 2-DOF mirror-scanner toward a MO to be focused at the petri dish glass-water interface. The laser absorption generates localized thermocapillary convection flow that drags the bead toward the laser focus. A high speed camera monitors this process.

Before inserting microparticles into the petri dish, a quantity of distilled water was added to obtain a pre-determined depth. This depth was measured by focusing the microscope objective first at the glass-water interface and then at the water-air interface. Next, particles were carefully deposited onto the water surface. A droplet was then carefully taken from the sample using a pipette and dropped onto the particles.

In Vela et al. (2008), the feasibility of handling beads of any shape and composition in the size range from 30–300 μm was demonstrated. However, no velocity measurements or force estimates were performed for the Marangoni convection. In the next section, results of velocity measurements for immersed glass beads ranging in diameter from 31 up to 92 μm and in contact with the petri dish surface are presented.

Figure 3 shows an image sequence with its associated image processing for bead velocity measurements. A glass bead was placed at a specified distance (about

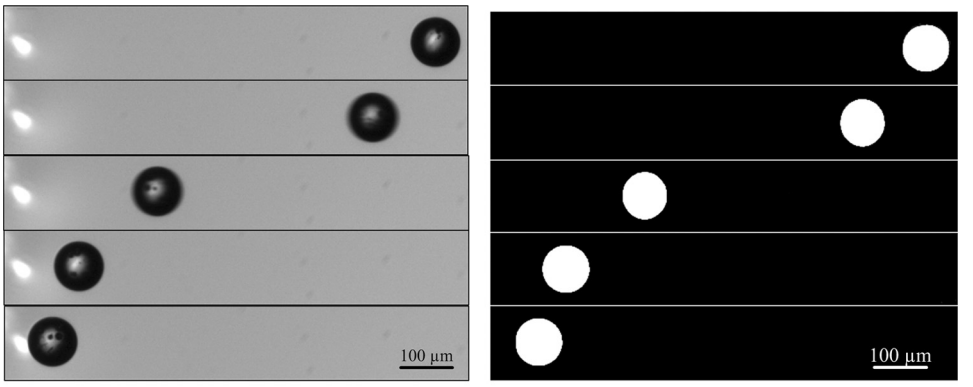

(*a*) (*b*)

Figure 3. Image sequences for velocity measurements of a spherical glass bead with 92 μm in diameter and within 600 μm of water depth. One image every 212.5 ms is shown. (*a*) Sequence taken at 80 Hz and (*b*) Image processing to determine the velocity field between the laser and bead. The mass center is obtained from the white region for each image, and then the distance between two successive mass center is computed and multiplied by the frame rate. Scale bar 100 μm.

800 μm) from the laser focus. The laser was then switched on in a continuous mode and switched off once the glass bead reached the laser. When the IR laser was on, the bead moved toward the laser focus (white region in Figure 3*a*) and came to a stop close to the focal point. The glass bead's displacement was monitored with a high speed CMOS camera. An image sequence of the bead motion was taken at a frame rate of 80 Hz. The images were processed (Figure 3*b*), one by one, to determine the distance and velocity field between the bead's center of mass and the laser focal point. Once this was determined, the velocity was computed by multiplying the difference between two successive center-of-mass positions and the frame rate. Each measurement shown is the mean of ten measurements.

4. RESULTS AND DISCUSSIONS

Figure 4 depicts the radial velocity field of a glass bead of diameter 92 μm, immersed in water and in contact with the petri dish surface. The zero point of the x axis corresponds to the focal point of the laser. Since Marangoni convection depends on the liquid depth, the smaller the depth the larger the velocity flow. Three different water depths of 375, 450, and 600 μm were investigated.

As shown in Figure 4, the bead velocity field increases with decreasing the water depth. This is due to the increase of the temperature gradient at the water-air interface, as more energy from the laser beam reaches this interface (the absorption coefficient, 2345/m, leads to a laser penetration of about 425 μm).

An increase in the temperature gradient causes an increase in the velocity gradient (c.f. Eq. (2)). We can see that the bead velocity first increases before reaching a maximum, after which it starts to decrease as it approaches the laser focal point. This can be explained by the fact that convective cells which are generated around the laser focal point, increase close to this point and decrease at a certain distance away from the focus. The flow momentum, therefore, changes from radial

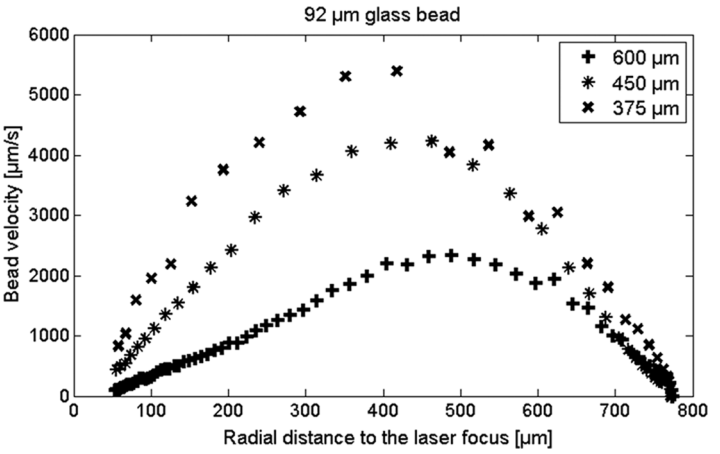

Figure 4. Velocity of a glass bead with 92 μm in diameter versus the radial distance of the bead center to the laser focus (origin) within three different water depths.

to vertical momentum; having a maximum radial momentum between the flow up and down positions. Consequently, when approaching the laser focal point the bead loses radial velocity and finally stops. A comparison between the velocity fields of different bead sizes is depicted in Figure 5 for 375 and 450 μm water depths. Figure 5*a* shows that the bead velocity depends on the bead size for a given water depth (450 μm). As seen on the velocity profile in Figure 1*b*, the bead velocity depends on the bead size. The larger the bead the larger the velocity profile reaching its surface. The drag force is also larger, and a larger bead will be heavier. However, at this scale surface effects are dominant over inertial effects and the flow has a greater surface area to push against. For smaller beads, there is a smaller contact surface area with the flow and they may become completely immersed in the boundary layer, decreasing their velocity significantly.

An error bar is shown in Figure 6 for glass beads of 92 and 31 μm in diameter (the largest and smallest beads used for these measurements) in a water depth of 600 μm. The error was calculated as the standard deviation over ten measurements. We can see that the errors are larger for higher velocities. These errors are due to the bead initial positions errors with respect to the laser focal point. Figure 7 illustrates the maximum bead velocity for different bead sizes, 31, 45, 62, 71, 79, and 92 μm in diameter, in three different water depths 375, 450, and 600 μm, respectively. We notice that in all cases, the maximum velocity increases with decreasing the water depth. For a given depth, considering all of the different bead sizes, we see that the maximum bead velocity tends to decrease as the bead size gets smaller. The depths of water were initially increased by 75 μm and then 150 μm from 375 μm to lead 450 and 600 μm, in water depth, respectively. By taking the maximum peak velocity for a water depth of 375 μm as reference, a 92-micron bead exhibits a speed decrease of 21% and 54.8% as water depth increases from 375 μm to 450 μm and 600 μm, respectively. The velocity decrease is about 2.6 times when reducing the water depth by a factor of 2 (150 μm). For a 31 μm bead the speed decreases were about 16.8% and 42.4%, which means 2.5 times. For a 71 μm bead, the velocity

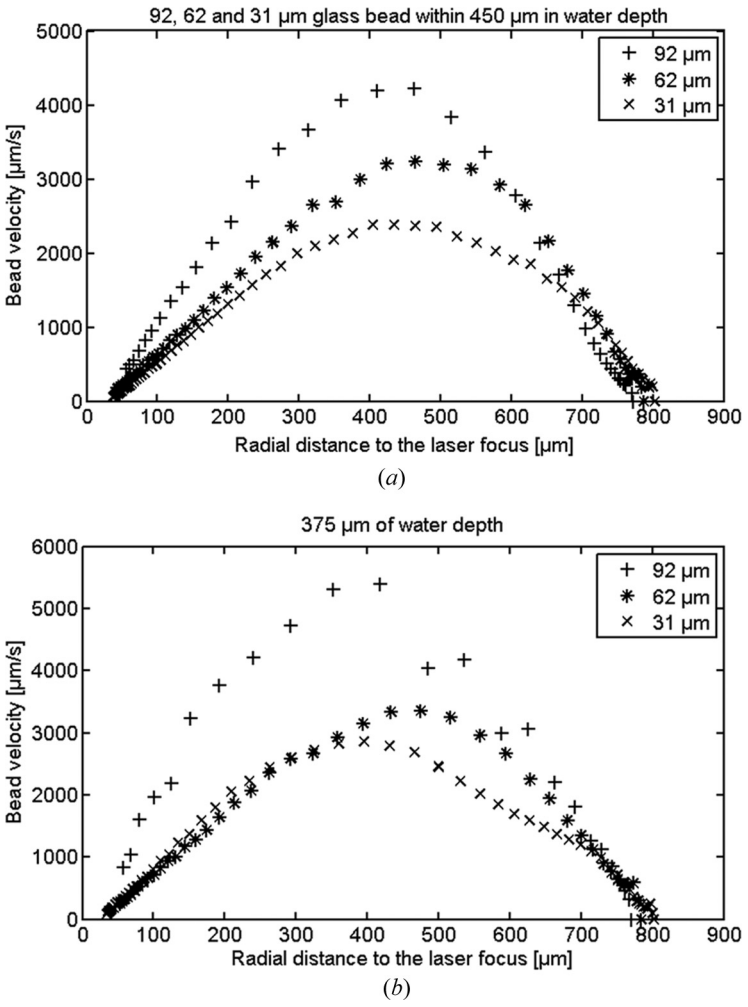

Figure 5. Velocity of three different glass beads with 92, 62, and 31 μm in diameter versus the radial distance to the laser focus. (*a*) Within 450 μm in water depth and (b) within 375 μm in water depth.

decrease is about 3 times. From Figure 7, we can conclude that if we increase the water depth by a factor of 2, the velocity for a constant bead size decreases between 2.5–3 times.

To estimate the force that the fluid is able to exert on a 92 μm-sized spherical bead in water depth 450 μm, we proceeded as follows. First, we assumed that the bead rolls (observed from experiments) to simplify the calculations. However, the bead can also slide. Then, a force analysis on the glass bead showed that $F_r = F_d - F_f$, where F_r, F_d, and F_f are the resultant forces on the bead due to its acceleration, the fluid force exerted on the bead and the friction force due to substrate-bead contact, respectively. Secondly, the bead accelerations (a_b) were calculated by taking the derivative of the experimental velocity field (c.f. Figure 4).

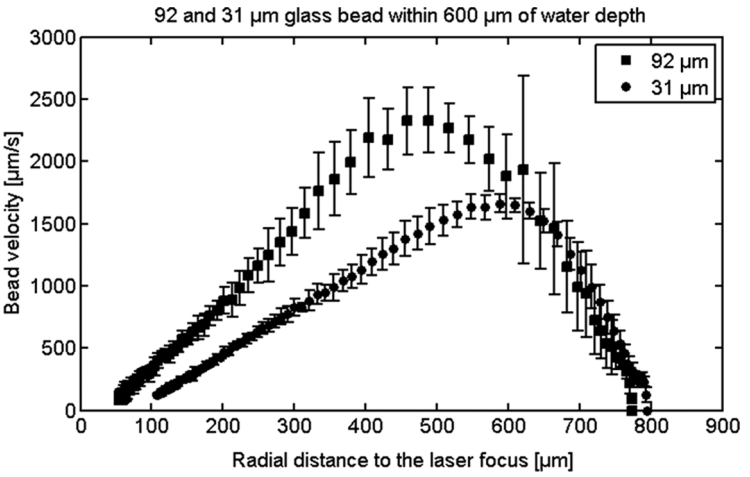

Figure 6. Velocity and error bar of a glass bead with 92 and 31 μm in diameter within 600 μm in water depth versus the radial distance to the laser focus. Error bar was calculated over ten measurements.

Knowing a_b, F_r is obtained from $F_r = ma_b = \rho_b V_b a_b$, where ρ_b and V_b are the density of the glass and the bead volume, respectively.

Finally, F_f is computed using $F_f = \gamma F_n$, where F_n is the normal force exerted on the bead, which is $F_n = (\rho_b - \rho)V_b g$ (difference between the bead weight and the Archimedes force). γ is the static friction coefficient for a glass-glass spherical bead contact in water ($\gamma = 0.227$) (Ishibashi et al. 1994). In Figure 8, the estimation of F_r and F_d are shown. The fluidic force, F_d, exerted on the bead attains a magnitude of about 1.4 nN.

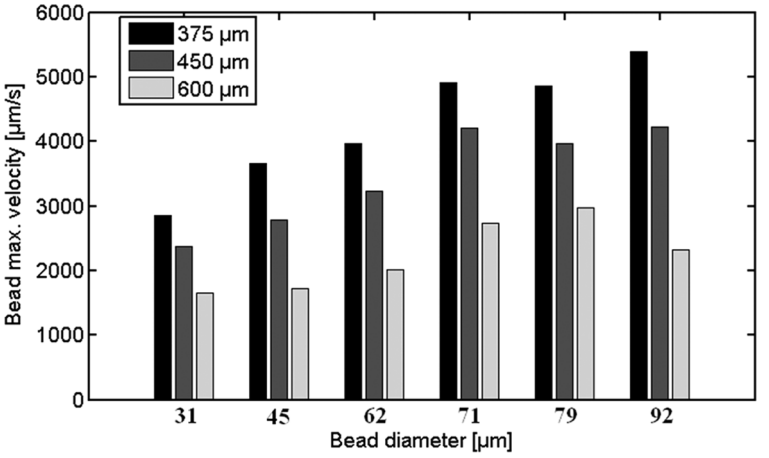

Figure 7. Peak velocity of glass beads 31, 45, 62, 71, 79, and 92 μm in diameter, respectively, for three different water depth of 375, 450, and 600 μm.

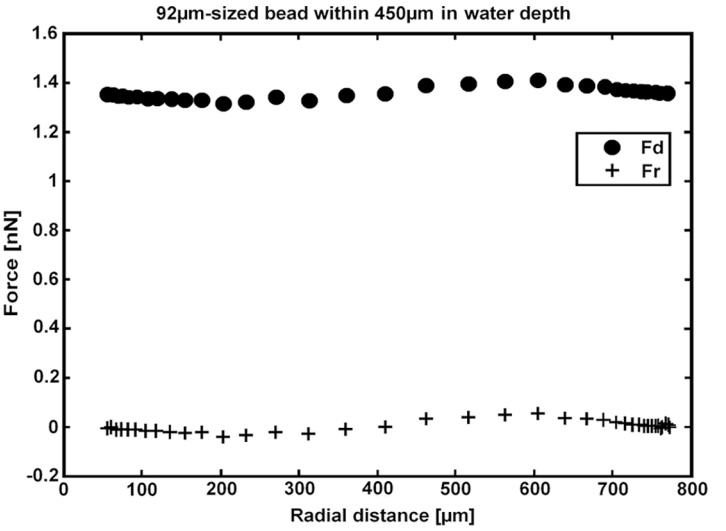

Figure 8. Estimation of the force F_d exerted by the fluid on a 92 µm-sized glass bead. F_r represents an estimation of the resultant force due to the bead acceleration.

5. CONCLUSION

A mesoscale manipulation technique for large and random-shaped beads was successfully developed using Bénard-Marangoni convection flow. A focused 1480 nm IR laser was used to locally heat a thin liquid layer of distilled water and to generate localized convection flow. This permitted manipulation without the need for patterned or microfabricated substrates. A simple petri dish was filled with liquid water to a predetermined depth (<0.8 mm).

Velocity measurements of glass beads (ranging from 31 to 92 µm in diameter) were performed with a high speed CMOS camera. Results showed that the largest glass bead (92 µm in diameter) was dragged at about 5.5 mm/s in 375 µm water depth. It appeared that the bead velocity depends on the bead size. The larger the size, the larger the velocity because the flow velocity profile on its surface is larger. For smaller beads the velocity profile decreases due to the boundary layer at the substrate-water interface.

The bead velocities also depend on water depth; the smaller the water depth, the higher the bead velocity. The manipulation velocity could be controlled to handle particles by adjusting the water depth. By scanning the IR laser with a high-speed scanner, we could modulate the surface tension, thus generating several kinds of patterns. These patterns could be selected to match the type of single or parallel manipulation desired, such as stirring, sorting, or precise handling. Future work will address vision feedback in order to achieve a fully automated system.

Automation of the presented system would be a significant and promising development for mesoscale manipulation, providing a versatile, cost-effective, and safe system (with respect to the temperature at the focal point, for example, for biological cells manipulation). Micron-sized beads could be dragged in parallel at high velocity (as demonstrated by the velocities observed in the

mm/s range) and in a safe temperature region. Future work will address temperature measurements in order to acquire a better understanding of the thermal distributions.

ACKNOWLEDGMENTS

Funding for this project was provided by the European GOLEM project, Bio-inspired Assembly Process for Mesoscale Products and Systems, FP 6, NMP, contract No. STRP 033211 (http://www.golem-project.eu/). The authors gratefully acknowledge OCTAX Microscience GmbH for providing the laser shot system and for the constructive discussions on the laser-liquid medium interactions.

REFERENCES

Adamson, A. W. and A. P. Gast. 1997. *Physical chemistry of surfaces*. 6th ed. New York: John Wiley and Sons.

Arai, Fumihito, Keiichi Yoshikawa, Toshihiro Sakami, and Toshio Fukuda. 2004. Synchronized laser micromanipulation of multiple targets along each trajectory by single laser. *Applied Physics Letters* 85(19):4301.1–4301.3.

Assi, Fabiano, Robert Jenks, Jerry Yang, Christopher Love, and Mara Prentiss. 2002. Massively parallel adhesion and reactivity measurements using simple and inexpensive magnetic tweezers. *Journal of Applied Physics* 92(9):5584–5586.

Baroud, Charles N., Jean-Pierre Delville, Francois Gallaire, and Régis Wunenburger. 2007. Thermocapillary valve for droplet production and sorting. *Physical Review E* 75(2):046302.1–046302.5.

Basu, Amar S. and Yogesh B. Gianchandani. 2007. Shaping high-speed marangoni flow in liquid films by microscale perturbations in surface temperature. *Applied Physics Letters* 90(3):034102.1–034102.3.

Basu, Amar S. and Yogesh B. Gianchandani. 2008. Virtual micro fluidic traps, filters, channels and pumps using marangoni flows. *Journal of Micromechanics and Microengineering* 18(11):115031.1–115031.11.

Chiou, Pei Yu, Aaron T. Ohta, and Ming C Wu. 2005. Massively parallel manipulation of single cells and microparticles using optical images. *Nature Letters* 436(7049):370–372.

Chung, Su Eun, Wook Park, Sunghwan Shin, Seung Ah Lee, and Sunghoon Kwon. 2008. Guided and fluidic self-assembly of microstructures using railed microfluidic channels. *Nature Materials* 7(7):581–587.

Cordero, Maria Luisa, Daniel R. Burnham, Charles N. Baroud, and David McGloin. 2008. Thermocapillary manipulation of droplets using holographic beam shaping: Microfluidic pin ball. *Applied Physics Letters* 93(3):034107.1–034107.3.

Curtis, J. E., B. A. Koss, and D. G. Grier. 2002. Dynamic holographic optical tweezers. *Optics Communications* 207(1):169–175.

DaCosta, German. 1993. Optical visualization of the velocity distribution in a laser-induced thermocapillary liquid flow. *Applied Optics* 32(12):2143–2151.

Darhuber, Anton A. and Sandra M. Troian. 2005. Principles of microfluidic actuation by modulation of surface stresses. *Annu Rev Fluid Mech* 37:425–455.

Darhuber, Anton A., Joseph P. Valentino, Sandra M. Troian, and Sigurd Wagner. 2003. Thermocapillary actuation of droplets on chemically patterned surfaces by programmable microheater arrays. *Journal of Microelectromechanical Systems* 12(6):873–879.

Haliyo, D. S., F. Dionnet, and S. Régnier. 2006. Controlled rolling of micro-objects for autonomous manipulation. *International Journal of Micromechatronics* 3(2):75–101.

Hollis, Artha, Sohi Rastegar, Laurent Descloux, Guy Delacréttaz, and Klaus Rink. 1996. Analysis of dynamics of zona pellucida microdrilling by a 1.48 μm diode laser. *IEEE Engineering in Medicine and Biology Society*, 2059–2060.

Ishibashi, I., C. Perry, III., and T. K. Agarwal. 1994. Experimental determinations of contact friction for spherical glass particles. *Soils and Foundations* 34(4):79–84.

Kataoka, Dawn E. and Sandra M. Troian. 1999. Patterning liquid flow on the microscopic scale. *Nature* 402(6763):794–797.

Lambert, P. and S. Régnier. 2006. Surface and contact forces models within the framework of microassembly. *International Journal of Micromechatronics* 3(2):123–157.

Longtin, Jon P., Kunio Hijikata, and Kuniyasu Ogawa. 1999. Laser induced surface tension driven flows in liquids. *International Journal of Heat and Mass Transfer* 42(1):85–93.

Maroto, J. A., V. Pérez-Munuzuri, and M. S. Romero-Cano. 2007. Introductory analysis of Bénard-Marangoni convection. *European Journal of Physics* 28(2):311–320.

Millet, O., P. Bernardoni, S. Régnier, Ph. Bidaud, D. Collard, and L. Buchaillot. 2004. Electrostatic micro-gripper coupled to an amplification mechanism. *Sensors and Actuators A: Physics* 114(2–3):371–378.

Moesner, Felix M. and Toshiro Higuchi. 1997. Contactless manipulation of microparts by electric field traps. *SPIE's International Symposium on Microrobotics and Microsystem Fabrication* 3202:168–175.

Ohta, Aaron T., Arash Jamshidi, Justin K. Valley, Hsan-Yin Hsu, and Ming C. Wu. 2007. Optically actuated thermocapillary movement of gas bubbles on an absorbing substrate. *Applied Physics Letters* 91(7):074103.1–074103.3.

Pollack, Michael G., Richard B. Fair, and Alexander D. Shenderov. 2000. Electrowetting-based actuation of liquid droplets for microfluidic applications. *Applied Physics Letters* 77(11):1725–1726.

Ramsay, William and John Shields. 1893.The molecular complexity of liquids. *Journal of Chemical Society* LXXXI:1089–1103.

Squires, Todd M. and Stephen R. Quake. 2005. Microfluidics: Fluid physics at the nanoliter scale. *Reviews of Modern Physics* 77(3):977–1026.

Vela, E., C. Pacoret, S. Bouchigny, S. Régnier, K. Rink, and A. Bergander. 2008. Non-contact mesoscale manipulation using laser induced convection flows. *IEEE/RSJ International Conference on Intelligent Robots and Systems*, September:913–918.